THE JOURNAL OF PHYSICAL CHEMISTRY LETTERS
A JOURNAL OF THE AMERICAN CHEMICAL SOCIETY

pubs.acs.org/JPCL Letter

# Overcoming Inaccuracies in Machine Learning Interatomic Potential Implementation for Ionic Vacancy Simulations

Pandu Wisesa and Wissam A. Saidi*

Cite This: J. Phys. Chem. Lett. 2025, 16, 31−37 Read Online

ACCESS | Metrics & More | Article Recommendations | Supporting Information

**ABSTRACT:** Machine learning interatomic potentials, particularly ones based on deep neural networks, have taken significant strides in accelerating first-principles simulations, expanding the length and time scales of the simulations with accuracies akin to first-principles simulations. Notwithstanding their success in accurately describing the physical properties of pristine ionic systems with multiple oxidation states, herein we show that an implementation of deep neural network potentials (DNPs) yield vacancy formation energies in MgO with a significant ∼3 eV error. In contrast, we show that moment tensor potentials can accurately describe all properties of the oxide, including vacancy formation energies. We show that the vacancy formation energy errors in DNPs correlate with the strength of ionic interactions in the system as evidenced by contrasting MgO with the less ionic systems $Cu_xO_y$ and $Ag_xO_y$. Our findings suggest that descriptors employed in the DNP may be inadequate and cannot accurately describe vacancies in ionic systems.

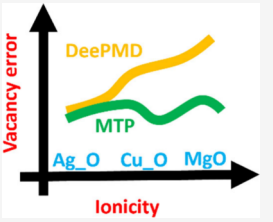




The high fidelity of first-principles calculations accelerates the digital discovery and design of materials.[1−3] However, this approach typically requires significant computational resources that limit its applicability for large simulations, which have on the order of thousands of atoms and for time scales beyond nanoseconds. To enable the design of increasingly complex materials, such as high entropy materials,[1,2,4] and to simulate more complex conditions, e.g., alloy−oxide interfaces and extreme environments, there is a need to have an accompanying or alternative approach that can achieve similar accuracy but with less computational resources. To this end, machine learning interatomic potentials (MLIAPs) are emerging as a new frontier in materials modeling at the atomic scale that can accelerate first-principles modeling by orders of magnitude while retaining high-fidelity quality simulations.[5]

In a recent study, we highlighted MLIAP's capability to describe pristine binary metal oxides.[6] Specifically, we trained deep neural network potentials (DNPs) using DeePMD-kit[7,8] for $A_xO_y$ (A = Cu, Mg, Ag, Pt, Zn) and found that each potential can successfully replicate basic physical properties of the oxides, such as cohesive energies, lattice constants, elastic constants, and surface energy with an accuracy akin to first-principles methods.[6] This finding was noteworthy given the multivalent nature of each oxide and the different lattice symmetries, e.g., the $Ag_xO_y$ DNP was able to describe well two AgO polymorphs, monoclinic ($P2_1/c$) and orthorhombic ($Cccm$), cubic $Ag_2O$ ($Pn\bar{3}m$), and monoclinic $Ag_3O_4$ ($P2_1/c$). With further training, e.g., for MgO, the DNP replicated DFT results in thermal expansion,[6] even the phase transition at extreme pressures and temperatures.[9] In our efforts to design DNPs for oxides[6] as well as for pure metals,[10−13] we focused on designing compact training data sets that can be used as a stepping-stone for the community to utilize in additional investigations (all databases and potentials can be found on our GitHub page[14]).

As the aim of MLIAPs is to help bridge the gap between DFT scales and experiments,[15] there is a need for these frameworks to successfully describe vacancies that are omnipresent in materials. For instance, even under ideal synthesis conditions leading to pristine materials with no defects, it can be expected at nonzero temperatures from entropic considerations that a bulk material will contain a finite concentration of vacancies.[15] In our previous studies on metals and alloys, MLIAPs based on DNPs were able to successfully describe vacancies with high fidelity.[10,13,16] However, to our knowledge, MLIAPs have not been extensively utilized to describe vacancies in ionic systems, which unlike metallic systems could pose a challenge owing to the nature of ionic interactions in the system.

Herein, we show that DNPs based on DeePMD-kit,[7,8] as employed in our previous study,[6] fail to correctly describe the neutral oxygen and magnesium vacancies in binary oxides despite extensive extensions of the training data set. We show that the moment tensor potential (MTP) as implemented in the MLIP[17] package, in contrast, can provide a framework for accurately modeling the oxides including vacancies. We systematically explore the underpinnings of these findings and how they relate to the ionic nature of the interactions of the system. Our findings suggest that descriptors of atomic

Received: October 10, 2024
Revised: November 21, 2024
Accepted: November 26, 2024
Published: December 18, 2024

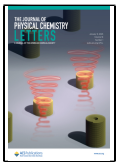





https://doi.org/10.1021/acs.jpclett.4c02934
J. Phys. Chem. Lett. 2025, 16, 31−37

environments as employed in MTP can be a viable approach for describing ionic systems with DNP without resorting to more complex and expensive computational approaches.

In our previous study, we created and validated DNPs to model various properties of metal oxides $Ag_xO_y$, $Cu_xO_y$, $Mg_xO_y$, $Pt_xO_y$, and $Zn_xO_y$ with different oxidation states and importantly without additional charge information, while utilizing a minimal data set with less than ∼4000 configurations per oxide. Further, we showed that these data sets can be augmented to enhance the DNP transferability, e.g., as demonstrated for a new polymorph, surface energies, and thermal expansion, or even in modeling the liquid phase of the oxide at extreme pressures up to ∼300 GPa.[6,9]

Using the $Mg_xO_y$ data set and focusing on the rock salt cubic phase, we find that the initial DNP has substantial errors in excess of few eV for calculating neutral O and Mg vacancy formation energies. We attributed this deficiency to the lack of explicit vacancy configurations in the data set. To address this, we applied an adaptive training approach similar to our previous protocol[6,9] targeting specifically vacancy configurations by adding 7214 new configurations (an ∼20% increase compared to the original 44,792). However, the DNP still failed to accurately describe the vacancy formation energies. Notably, we find that the error in the vacancy formation energy was, respectively, 1.9 and 2.0 eV for the O and Mg vacancies for the 1 × 1 × 1 conventional unit cell with eight atoms. The variation of the vacancy formation energies with different supercells is summarized in Figure 1 and compared to DFT

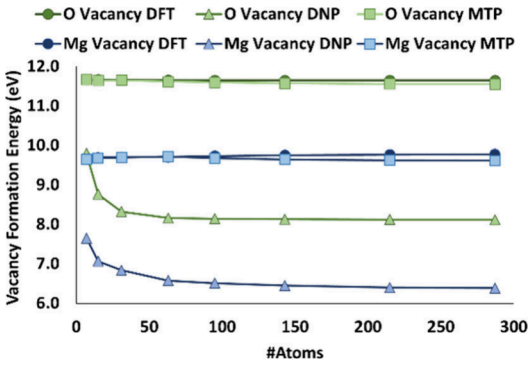


**Figure 1.** Vacancy formation energy as a function of system size for MgO with O vacancy (green) and Mg vacancy (blue) as obtained based on DFT (circle), DNP (triangle), and MTP (square). The smallest supercell 1 × 1 × 1 contains eight atoms and the largest one 3 × 3 × 4 has 288 atoms.

values. Significantly, the figure illustrates that for the 3 × 3 × 4 supercell containing 288 atoms, the vacancy formation energy in the dilute limit converges to values with errors of 3.5 eV for O and 3.4 eV for Mg relative to DFT calculations.

To ensure that this finding is not an artifact of the training data set, we carried out two additional training computational experiments. First, using the data set developed so far with 52,006 configurations, we developed a DNP after adding 5696 configurations with O and Mg vacancies based on molecular dynamics (MD) simulations for a 2 × 2 × 2 supercell. The DNP results with the new potential, after retraining, however, still displayed significant errors. In particular, the 2 × 2 × 2 supercell that was specifically targeted in the new training protocol had substantial errors of 3.0 and 3.4 eV for O and Mg vacancy formation energies, respectively. In the second experiment, we trained a set of potentials using only the vacancy configurations, which amounts to 12,910 configurations. This set is nearly 3 times the size of the data set utilized to train a DNP that can describe the basic physical properties of the pristine binary oxide with high accuracy.[6] While this process allowed for a slight reduction in error (the error decreased, respectively, by 0.6 and 0.7 eV for O and Mg), the average error for both vacancy types is still over ∼2 eV. The persistent nature of these energy values is shown in Figure S1.

Due to the nature of deep neural networks, it is difficult to identify the cause of the divergence by DNPs from DFT results. Our investigations ruled out that this could be due to the inadequacy of the computational framework adopted to develop the training database. For instance, the DNP properties of pristine MgO agree well with DFT (Table S1). Also, the DFT vacancy formation energies are also consistent with previous studies.[18] We thus posit that the descriptors employed in the DNP may be inadequate and cannot accurately describe vacancies in ionic systems.

To provide more insight, we investigated applying an alternative MLIAP based on the moment tensor potentials (MTPs), as implemented in MLIP.[17,19] There are some notable differences between the two MLIAPs. Both MLIAPs employ implementations of atomic descriptors that account for all of the angular and radial information in the local atomic environment. The two methods differ, however, in their regressor, where the DNP employs a multilayered deep neural network while the MTP is based on linear regression with a set of basis functions. Additionally, the active learning mechanism employed to train the model error is also different between the two methods, though not expected to impact the fidelity of the potential. Specifically, the DNP utilizes an ensemble of potentials that acts as a committee that "votes" for energy, force, and stress of a given atomic environment.[20] The deviation of these votes indicates a level of disagreement, which pinpoints the new information that is needed to be supplemented into the data set. On the other hand, the MTP employs D-optimality criterion,[21] which is a geometric prescription to determine the extent of distinctness of a given configuration compared to the ones existing in the data set.[17]

Figure 2 shows the employed protocol in developing the MTPs for the oxides (see the Methodology section for further details). To assess the quality of the resulting MTPs, we compared the MTP performance to that of DFT and DNP on different properties of the system. Table S1 shows that MTP performs equally to DNP in replicating DFT values. Importantly, and in contrast to the DNP results, the MTP and Mg vacancy formation energies are very close to the corresponding DFT values with ∼0.05 eV deviations, as shown in Figure 1. We note that the MgO MTP is trained on only 1231 configurations (including configurations with vacancies), which is a fraction of the data set size used with the DNP. As a further validation, we also examined finite size effects on vacancy formation energies by increasing the supercell size up to 10 × 10 × 10 (8000 atoms). As shown in Figure S2, the MTP formation energies are already well-converged with 2 × 2 × 2 supercells (64 atoms) consistent with DFT (see Figure 1).

The MgO MTP is further examined in simulating a more complex property, namely, thermal expansion, to contrast with similar investigations obtained using the DNPs.[6,9] Since the MTP was already trained in MD simulations with an NPT


https://doi.org/10.1021/acs.jpclett.4c02934
J. Phys. Chem. Lett. 2025, 16, 31−37

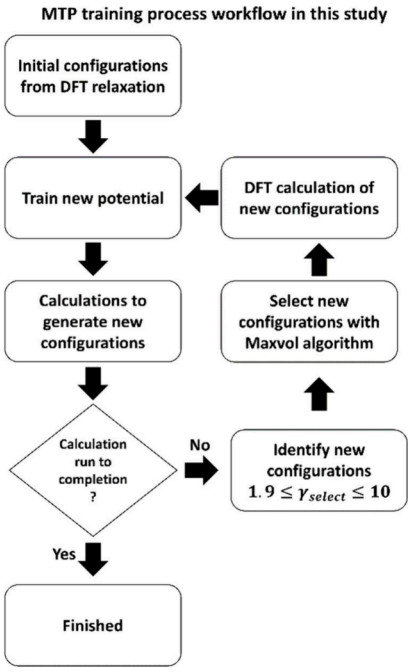


**Figure 2.** The MTP training process employed in this study. See the Methodology section for further details.

(constant pressure, temperature) ensemble, we did not add an additional active learning process and it was utilized as is for this investigation. Figure 3 shows that the MTP results (green

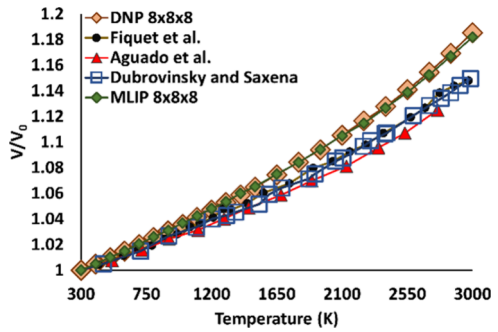


**Figure 3.** Relative expansion of MgO from room temperature as a function of temperature. Orange diamonds represent DNP results,[6] green diamonds represent MTP from this study, blue markers are from Dubrovinsky and Saxena,[23] green markers are from Aguado et al.,[25] and yellow markers are from Fiquet et al.[24]

diamonds) overlap with those of DNP (orange diamonds), indicating that both methods perform similarly in the thermal expansion of the pristine system. Notably, as shown in Figure 3, the MTP and DNP potentials capture the nonharmonic behavior as temperature increases,[22−24] in agreement with other studies.[23−25]

Our findings clearly show that the MTP approach can successfully replicate all previous results for the MgO system that were obtained with the DNP approach and further is also able to describe with high fidelity the formation energies of the O and Mg vacancy formation energies. To ensure that these results are not specific to MgO, we also investigated two additional binary metal oxides $Cu_xO_y$ and $Ag_xO_y$. For $Cu_xO_y$, we included two CuO polymorphs, orthorhombic (*Cccm*) and tetragonal ($P4_2/mmc$), along with $Cu_2O$ ($Pn\bar{3}m$). The $Ag_xO_y$ included two AgO polymorphs, monoclinic ($P2_1/c$) and orthorhombic (*Cccm*), cubic $Ag_2O$ ($Pn\bar{3}m$), and monoclinic $Ag_3O_4$ ($P2_1/c$). These structures were selected to observe trends for different charge states, lattices, and polymorphs along with contrasting the results between different metal atoms.

Similarly to the MgO case, we began with the existing DNP for $Cu_xO_y$ and $Ag_xO_y$ that we had previously developed, which includes ∼7.4k configurations. To capture environments specific to vacancies, we employed an active learning protocol, adding respectively 21,145 and 14,561 vacancy configurations to $Cu_xO_y$ and $Ag_xO_y$ databases, with a variety of supercell sizes from unit cell to 3 × 3 × 3. Here, we significantly expanded the data set size, as our goal is to develop an optimal DNP with enhanced accuracy, placing less emphasis on the compactness of the data set.[6] Further, using the same protocol discussed in Figure 2 for MgO, we also developed MTPs using 2449 and 3267 configurations for $Cu_xO_y$ and $Ag_xO_y$, respectively, including configurations with vacancies. As shown in Figure S6 and Tables S2 and S3, the MTP results for several physical properties of the oxides are in very good agreement with those obtained with DFT and DNP.

Figure 4 summarizes the MLP and DNP vacancy formation energies as a radar chart of error vs DFT where the area in the

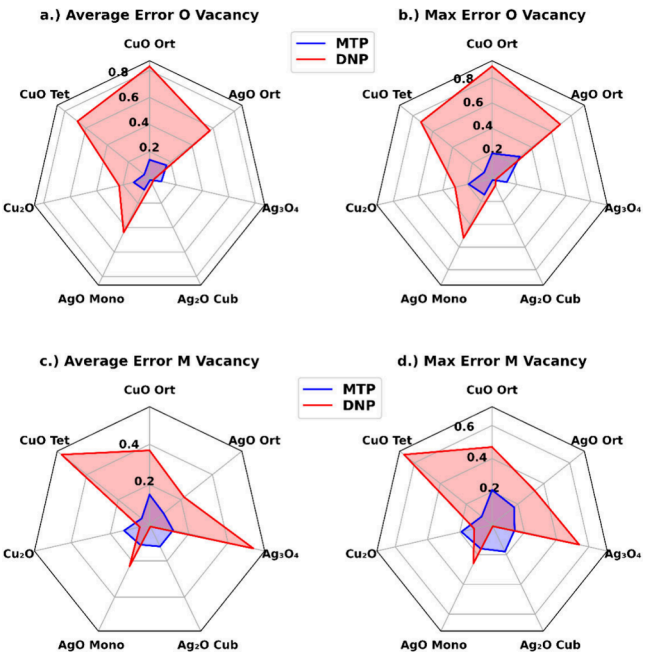


**Figure 4.** Radar chart of error vs DFT values for MTP (blue) and DNP (red) for $Cu_xO_y$ and $Ag_xO_y$. The average and max error (a and b) for O vacancies and (c and d) for Mg vacancies. The area in the radar plots correlates with the error, where smaller area is indicative of smaller errors. All values are in eV.

radar plot is indicative of accuracy. To capture both trend and largest error outliers, we present the average and maximum errors for formation energies over 2 × 2 × 2 (24 atoms) to 3 × 3 × 4 (288 atoms) supercells. As can be observed in Figures S4 and S5, the $Ag_xO_y$ and $Cu_xO_y$ DFT vacancy formation energies tend to flatten out for system sizes beyond the 2 × 2 × 2 supercell size. Also, we note that because the primitive unit cell of the smallest system may consist of as few as four atoms, we


https://doi.org/10.1021/acs.jpclett.4c02934
J. Phys. Chem. Lett. 2025, 16, 31−37

opted to exclude supercell sizes smaller than 2 × 2 × 2 to avoid unphysical systems.

Compared to MgO, the DNP fidelity is appreciably better for $Cu_xO_y$ and $Ag_xO_y$ as none of the red radar in Figure 4 exceeds 0.8 eV. Scrutinizing Figure 4 further, it is interesting to note that the DNP performs best for oxides with more complex oxidation states, i.e., $Ag_2O$, $Cu_2O$, and $Ag_3O_4$, and worse for AO (A = Ag, Cu) regardless of lattice, albeit the Ag vacancy in $Ag_3O_4$ is an outlier in this trend. On the other hand, the MTP does not seem to be affected by the oxidation state of the oxides and overall does not seem to have appreciable difficulty in replicating the energetics from the DFT calculations, as indicated by the small radar area. The raw numbers for all of the data points can be found in Tables S4 and S5. A slightly different way to observe this comparison is through a parity plot, as shown in Figure S3.

The differences in the DNP performance among the three different oxides are notable. To better understand these differences, we performed Bader charge analysis[26−28] to quantify the degree of ionicity for each solid; the results can be found in Table 1. While the Bader charge values are not absolute given the ambiguities of charge decomposition schemes in DFT, the analysis still provides a means of comparison of the ionicity for any given vacancies. Our DNP results show that the largest error in vacancy formation energy is for MgO (∼3 eV), and we observe that this system is also the most ionic out of the three investigated oxides. In contrast, $Cu_xO_y$ and $Ag_xO_y$ are at least ∼50% less ionic, which is consistent with the smaller observed DNP errors in the vacancy formation energies for these systems.

**Table 1. Bader Charge Analysis of the Pristine Binary Oxides**

| binary oxide | average electron donated to oxygen (contribution per metal atom) |
|---|---|
| MgO | 1.54 |
| CuO (ort) | 0.95 |
| CuO (tet) | 0.95 |
| $Cu_2O$ | 1.05 (0.525) |
| AgO (mono) | 0.83 |
| AgO (ort) | 0.82 |
| $Ag_3O_4$ | 0.77 (1.03) |
| $Ag_2O$ | 0.94 (0.47) |

From the point of view of electron transfer per metal atom, binary oxides with more complex oxidation systems tend to involve electron contributions from multiple metal atoms. For instance, per primitive cell, the 1.05 electrons transferred to O in $Cu_2O$ originate from two different Cu atoms, as opposed to CuO, where it originates from one Cu atom; similar arguments are applicable for $Ag_2O$. $Ag_3O_4$ offers a more complex case, as the total 0.77 electrons that each O receives requires 1.03 electrons transferred from each Ag atom. The larger amount of electrons transferred from the Ag atom may be related to the higher error for the Ag vacancy formation energy for $Ag_3O_4$ compared to the $Ag_xO_y$ systems. Hence, instead of the complexity of the oxide, the extent of the electrons transferred per metal atom may correlate to the extent of the error in the vacancy formation energy. On the other hand, such correlation is not as apparent from the perspective of the oxygen atom. For instance, $Ag_2O$, whose oxygen atoms receive more electrons than the AgO polymorphs, has a lower O vacancy energy error. Hence, correlations, if any, between the amount of electrons accepted by the oxygen atoms and the DNP errors observed in the vacancy formation energies are not as clear. Due to the simplicity of this analysis, performing Bader charge analysis on a unit cell of a material of interest could still be a useful and inexpensive approach to assess the fidelity of the DNP prior to performing any training.

The DNP as implemented through the DeepMD-kit has multiple descriptor implementations for describing the atomic environment. To examine their impact, we examined other descriptors, namely, se_e2_a, se_e2_r, se_e3, and se_atten_v2,[8,29,30] as implemented in a new version of the code, DeepMD-kit 2.2.4.[8] The details of these descriptors can be found elsewhere in the developers' documentation.[31] We elected to focus on the $Ag_xO_y$ system as this system has the largest number of polymorphs and the DNP performed relatively better than the other oxides (Figure 4). We utilized the same $Ag_xO_y$ data set developed in this study for these investigations and utilized the same hyperparameters as in our previous studies[6,9−12,16] except for se_e3, as discussed below.

The vacancy formation energies for the DNPs with the different descriptors are summarized in Figure 5. Namely, to provide a quick summary of the results, we show the average errors with respect to the DFT values. The complete breakdown can be found in the SI containing all the raw data for all MLIAPs, supercell sizes, and vacancy types. Also, as comparative reference, we show the corresponding average errors for the MTP (green bar) and DNP (blue bar) based on the data in Figures S3c and S3d, which correspond to the bars in Figures 5a and 5b, respectively. The orange se_e2_a bars represent results from DNPs trained with DeepPot-SE,[29] but with the newer software version DeepMD-kit 2.2.4. The se_e2_r descriptor that only utilizes the radial information does not appreciably affect the performance for the O vacancy but is worse for the Ag vacancy, as shown by the gray bar in Figure 5b. The se_atten_v2 (pink bar) descriptor that employs an attention-based descriptor[30] performs better than the reference DNP for O vacancies, but similar to se_e2_r could not retain the performance advantage for Ag vacancy. The se_e3 descriptor (white bars) incorporates a three-body descriptor, which involves the most information about the atomic environments compared to the other DNP descriptors. Indeed, this improved descriptor allowed for more accurate potentials, exceeding the benchmark DNP and becoming closer to that of MTP. However, this higher fidelity of the DNP simulations comes at a steep increase in training costs and required a reduction in hyperparameter values. Specifically, for the DNP training with se_e3, we had to reduce the maximum cutoff from 7 to 6 and the maximum neighbors from 140 to 80. The increase in training cost is most conveniently described by the change in GPU time spent that increased by a factor of 17 (on the NVIDIA A100 GPU).

Following this result, we additionally trained DNPs for MgO and $Cu_xO_y$ with the se_e3 descriptor. While Figure 5c shows that this three-body descriptor significantly improved the $Cu_xO_y$ results similarly to the $Ag_xO_y$ system (Figure 5c), especially for the case of the O vacancies, this improvement did not carry over to MgO (Figure 5d). Indeed, as seen in the figure, any improvement in the vacancy formation energy for MgO is relatively small, less than 0.5 eV (Figure 5d). Thus, we conclude that utilizing the three-body descriptor can improve the vacancy formation energy only for binary oxides with a lesser degree of ionicity.


https://doi.org/10.1021/acs.jpclett.4c02934
J. Phys. Chem. Lett. 2025, 16, 31−37

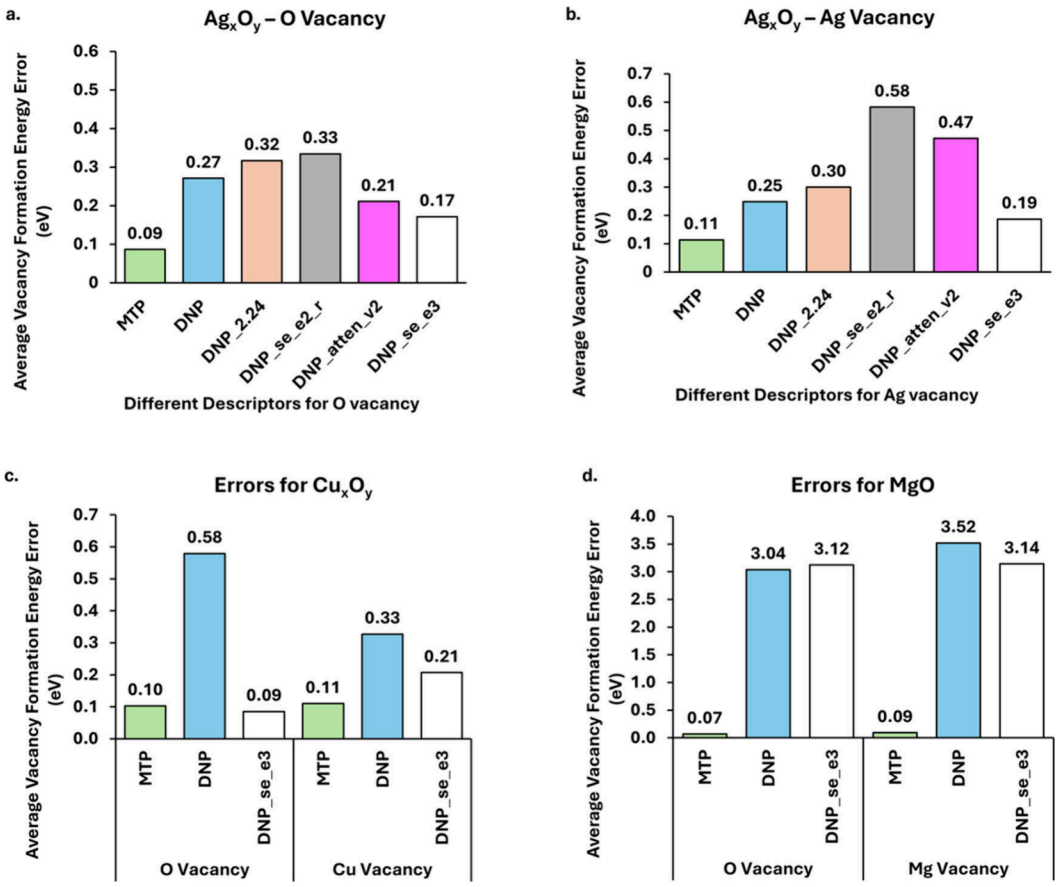


**Figure 5.** Average vacancy formation energy error for different MLIAPs and descriptors for (a) O vacancy and (b) Ag vacancy for supercells sized 2 × 2 × 2 and above. The comparison between MTP, DNP, and DNP_se_e3 for vacancies in (c) $Cu_xO_y$ and (d) MgO. The standard deviations of the averages are not included for clarity; the complete raw data can be found in Tables S4−S6.

We systematically investigated the performance of DNPs in describing vacancy formation energies in binary metal oxides. In particular, the standard DeepPot-SE as implemented in the DeepMD-kit has difficulty achieving high fidelities despite being proven to be robust for other properties of pristine oxides and also in metals and alloys including vacancy formation energies. Analyzing the trend in DNP error for each binary oxide through Bader charge analysis, we discovered that atoms that provide more ionic contribution correlate to larger errors when vacant. As such analysis is inexpensive relative to training a DNP, this approach is a good indicator that the resulting modeling can be explored prior to developing a DNP for vacancies. Further, we showed that the computationally costly three-body descriptor, se_e3, allows for some improvement, but only for the less ionic oxides.

Finally, we proposed the utilization of MTP as implemented in the MLIP package as an alternative solution. This diversification in the MLIAP approach provides a means to create MLIAPs that can describe physical properties equally well, while not encumbered by the same issue. Further MLIAPs that do not utilize neural networks tend to involve smaller data sets, which may translate to smaller computational resource requirements. Our findings suggest that descriptors employed in the DNP may be inadequate and cannot accurately describe vacancies in ionic systems.

## METHODOLOGY

DFT calculations were carried out using the Vienna *Ab Initio* Simulation Package (VASP).[32−34] The Kohn−Sham equations were solved within periodic boundary conditions with the Perdew−Burke−Ernzerhof (PBE)[35] exchange−correlation. Projector augmented wave (PAW)[34] was used to represent the electron−nucleus interactions in the pseudopotentials available with VASP.[36] The electronic cutoff was set to be 520 eV for all of the binary oxides. The Brillouin zone was sampled such that the smallest distance in the *k*-grid was set to be 0.24 $Å^{-1}$. The self-consistent electronic loop was set to terminate at a tolerance of at least $10^{-6}$ eV, sufficient convergence in physical properties for these systems.[6] The system investigated in this study is nonmagnetic as a perfect crystal, and similarly, the vacancy concentration in this study for relevant sizes, i.e., 2 × 2 × 2 and above, is insufficient to induce any meaningful magnetism.[37,38] Hence, all DFT calculations in this study are done without spin-polarization. Full relaxation on the atomic positions were performed for all configurations with vacancies.

Unless otherwise noted, all DNPs were developed using DeepMD-kit[7,8] version 2.0.3, which has proven to be robust for the previous oxide studies.[6,9] DeepPot-SE[29] descriptor is the standard descriptor, which was constructed from angular and radial information and is utilized in our previous studies.[6,9,11−13,16] A cutoff radius of 7 Å was used for neighbor searching, and 2 Å was set for the distance in which the smoothening starts. The embedding net was set to be 25 × 50 × 100 and the fitting net to be 240 × 240 × 240. The neural


https://doi.org/10.1021/acs.jpclett.4c02934
J. Phys. Chem. Lett. 2025, 16, 31−37

network was trained using the Adam stochastic gradient descent method that decreases exponentially from 0.001. The loss function prefactors for the energy, forces, and virials were kept at constant values of 1, 10,000, and 10, respectively. These parameters were found to be adequate and appropriate in our previous studies.[10−12,16] The DNP adaptive training follows the same protocol as discussed before.[6,9]

The MTP training process involves a learning-on-the-fly (LOTF) scheme, as depicted in Figure 2. This process involves the use of MD simulation with the NPT and NVE (constant volume and energy) ensembles along with a separate calculation on a 3 × 3 × 3 supercell to calculate the elastic constant using the finite difference method. The elastic constant calculations are specifically included to provide a small number of configurations with skews in different directions. The MD simulations were done on the relevant systems with cell sizes of 1 × 1 × 1, 1 × 1 × 2, 1 × 2 × 2, 2 × 2 × 2, 2 × 2 × 3, 2 × 3 × 3, and 3 × 3 × 3. The pristine system is only included as a unit cell. All other cell sizes consist of a system with a missing oxygen or metal atom. The training process is deemed complete when the NPT/NVE simulation can be fully carried out to 100 ps with no new configurations identified. The default weights of 1, 0.01, and 0.001 for energies, forces, and stresses, respectively, were chosen for the MTP. In our study, we chose the level of moments of 16 that has been shown to work well in various applications for solid state systems.[17] The potential cutoff of 7 Å is set the same as the DNP for consistency. The MTP package utilizes the extrapolation grade, $\gamma$, which determines the suitability of a given configuration with respect to the existing training data.[17] We used the default values for $\gamma$ as $2 \leq \gamma_{\text{select}} \leq 10$, where the upper bound of $\gamma$ is the break condition for a given iteration and the configurations with $\gamma$ in between are selected to be evaluated with DFT and included in the training set. The MgO MTP has an additional training scheme to ensure parity in thermal expansion comparison. The additional LOTF scheme involves NPT simulations at 500, 1000, 1500, 1900, 2000, 2250, 2700, 2850, and 3150 K at 0 pressure, and at 1, 5, 10, 30, 50, 100, 150, and 200 kbar at 2850 K. All atomistic calculations using the MLIAPs and DNPs were carried out using LAMMPS.[39]

## ■ ASSOCIATED CONTENT

### Supporting Information

The Supporting Information is available free of charge at https://pubs.acs.org/doi/10.1021/acs.jpclett.4c02934.

Document with a figure comparing vacancy formation for MgO for DNP trained with different data sets at increasing system size, a figure of MgO vacancy formation energy calculated with MTP from unit cell to a 10 × 10 × 10 supercell size, a set of parity plots of vacancy formation energy vs DFT for $Cu_xO_y$ and $Ag_xO_y$ systems, a set of figures showing the vacancy formation energy for $Ag_xO_y$ systems as a function of system size, a set of figures showing the vacancy formation energy for $Cu_xO_y$ systems as a function of system size, a parity plot of elastic constants of different MLIAPs compared to DFT, a $P-V$ plot at 2850 K for MgO as calculated by DNP and MTP, tables of physical property values as calculated with MLIAPs and DFT for MgO, $Cu_xO_y$, and $Ag_xO_y$ systems, and tables of raw values of vacancy formation energies at different system sizes for $Ag_xO_y$, $Cu_xO_y$, and MgO (PDF)

## ■ AUTHOR INFORMATION


### Corresponding Author

**Wissam A. Saidi** − *Department of Mechanical Engineering & Materials Science, University of Pittsburgh, Pittsburgh, Pennsylvania 15261, United States; National Energy Technology Laboratory, United States Department of Energy, Pittsburgh, Pennsylvania 15236, United States;* orcid.org/0000-0001-6714-4832; Email: alsaidi@pitt.edu

### Author

**Pandu Wisesa** − *Department of Mechanical Engineering & Materials Science, University of Pittsburgh, Pittsburgh, Pennsylvania 15261, United States;* orcid.org/0000-0001-8494-070X

Complete contact information is available at: https://pubs.acs.org/10.1021/acs.jpclett.4c02934


### Notes

The authors declare no competing financial interest.

## ■ ACKNOWLEDGMENTS

We are grateful to the U.S. National Science Foundation (Awards CSSI-2003808 and CBET-2130804). This research was supported in part by the University of Pittsburgh Center for Research Computing through the resources provided. Specifically, this work used the H2P cluster, which is supported by NSF Award OAC-2117681. Also, we acknowledge computational resources from Argonne Leadership Computing Facility, which is a DOE Office of Science User Facility supported under Contract DE-AC02-06CH11357.

## ■ REFERENCES


(1) Saidi, W. A. Emergence of Local Scaling Relations in Adsorption Energies on High-Entropy Alloys. *npj comput. mater.* **2022**, *8* (1), 86.

(2) Lederer, Y.; Toher, C.; Vecchio, K. S.; Curtarolo, S. The Search for High Entropy Alloys: A High-Throughput Ab-Initio Approach. *Acta Mater.* **2018**, *159*, 364−383.

(3) Emery, A. A.; Wolverton, C. High-Throughput Dft Calculations of Formation Energy, Stability and Oxygen Vacancy Formation Energy of Abo3 Perovskites. *Scientific Data* **2017**, *4* (1), 170153.

(4) Kaufmann, K.; Maryanovsky, D.; Mellor, W. M.; Zhu, C.; Rosengarten, A. S.; Harrington, T. J.; Oses, C.; Toher, C.; Curtarolo, S.; Vecchio, K. S. Discovery of High-Entropy Ceramics Via Machine Learning. *npj comput. mater.* **2020**, *6* (1), 42.

(5) Behler, J. Four Generations of High-Dimensional Neural Network Potentials. *Chem. Rev.* **2021**, *121* (16), 10037−10072.

(6) Wisesa, P.; Andolina, C. M.; Saidi, W. A. Development and Validation of Versatile Deep Atomistic Potentials for Metal Oxides. *J. Phys. Chem. Lett.* **2023**, *14* (2), 468−475.

(7) Wang, H.; Zhang, L.; Han, J.; E, W. Deepmd-Kit: A Deep Learning Package for Many-Body Potential Energy Representation and Molecular Dynamics. *Comput. Phys. Commun.* **2018**, *228*, 178−184.

(8) Zeng, J.; Zhang, D.; Lu, D.; Mo, P.; Li, Z.; Chen, Y.; Rynik, M.; Huang, L. a.; Li, Z.; Shi, S.; Wang, Y.; Ye, H.; Tuo, P.; Yang, J.; Ding, Y.; Li, Y.; Tisi, D.; Zeng, Q.; Bao, H.; Xia, Y.; Huang, J.; Muraoka, K.; Wang, Y.; Chang, J.; Yuan, F.; Bore, S. L.; Cai, C.; Lin, Y.; Wang, B.; Xu, J.; Zhu, J.-X.; Luo, C.; Zhang, Y.; Goodall, R. E. A.; Liang, W.; Singh, A. K.; Yao, S.; Zhang, J.; Wentzcovitch, R.; Han, J.; Liu, J.; Jia, W.; York, D. M.; E, W.; Car, R.; Zhang, L.; Wang, H. Deepmd-Kit V2: A Software Package for Deep Potential Models. *J. Chem. Phys.* **2023**, *159* (5), 054801.

(9) Wisesa, P.; Andolina, C. M.; Saidi, W. A. Machine-Learning Accelerated First-Principles Accurate Modeling of the Solid-Liquid Phase Transition in Mgo under Mantle Conditions. *J. Phys. Chem. Lett.* **2023**, *14* (39), 8741−8748.
(10) Andolina, C. M.; Williamson, P.; Saidi, W. A. Optimization and Validation of a Deep Learning Cuzr Atomistic Potential: Robust Applications for Crystalline and Amorphous Phases with near-Dft Accuracy. *J. Chem. Phys.* **2020**, *152* (15), 154701.
(11) Andolina, C. M.; Bon, M.; Passerone, D.; Saidi, W. A. Robust, Multi-Length-Scale, Machine Learning Potential for Ag−Au Bimetallic Alloys from Clusters to Bulk Materials. *J. Phys. Chem. C* **2021**, *125* (31), 17438−17447.
(12) Andolina, C. M.; Wright, J. G.; Das, N.; Saidi, W. A. Improved Al-Mg Alloy Surface Segregation Predictions with a Machine Learning Atomistic Potential. *Phys. Rev. Mater.* **2021**, *5* (8), 083804.
(13) Andolina, C. M.; Saidi, W. A. Highly Transferable Atomistic Machine-Learning Potentials from Curated and Compact Datasets across the Periodic Table. *Digital Discovery* **2023**, *2* (4), 1070−1077.
(14) Pandu Wisesa, C. M. A.; Saidi, W. A. https://github.com/saidigroup.
(15) Kim, S. J.; Kim, Y. I.; Lamichhane, B.; Kim, Y.-H.; Lee, Y.; Cho, C. R.; Cheon, M.; Kim, J. C.; Jeong, H. Y.; Ha, T.; Kim, J.; Lee, Y. H.; Kim, S.-G.; Kim, Y.-M.; Jeong, S.-Y. Flat-Surface-Assisted and Self-Regulated Oxidation Resistance of Cu(111). *Nature* **2022**, *603* (7901), 434−438.
(16) Bayerl, D.; Andolina, C. M.; Dwaraknath, S.; Saidi, W. A. Convergence Acceleration in Machine Learning Potentials for Atomistic Simulations. *Digital Discovery* **2022**, *1* (1), 61−69.
(17) Novikov, I. S.; Gubaev, K.; Podryabinkin, E. V.; Shapeev, A. V. The Mlip Package: Moment Tensor Potentials with Mpi and Active Learning. *Machine Learning: Science and Technology* **2021**, *2* (2), 025002.
(18) Gibson, A.; Haydock, R.; LaFemina, J. P. Stability of Vacancy Defects in Mgo: The Role of Charge Neutrality. *Phys. Rev. B Condens Matter* **1994**, *50* (4), 2582−2592.
(19) Shapeev, A. V. Moment Tensor Potentials: A Class of Systematically Improvable Interatomic Potentials. *Multiscale Model. Simul.* **2016**, *14* (3), 1153−1173.
(20) Artrith, N.; Behler, J. High-Dimensional Neural Network Potentials for Metal Surfaces: A Prototype Study for Copper. *Phys. Rev. B* **2012**, *85* (4), 045439.
(21) Podryabinkin, E. V.; Shapeev, A. V. Active Learning of Linearly Parametrized Interatomic Potentials. *Comput. Mater. Sci.* **2017**, *140*, 171−180.
(22) Reeber, R. R.; Goessel, K.; Wang, K. Thermal Expansion and Molar Volume of Mgo, Periclase, from 5 to 2900 K. *Eur. J. Mineral.* **1995**, *7* (5), 1039−1048.
(23) Dubrovinsky, L. S.; Saxena, S. K. Thermal Expansion of Periclase (Mgo) and Tungsten (W) to Melting Temperatures. *Phys. Chem. Miner.* **1997**, *24* (8), 547−550.
(24) Fiquet, G.; Richet, P.; Montagnac, G. High-Temperature Thermal Expansion of Lime, Periclase, Corundum and Spinel. *Phys. Chem. Miner.* **1999**, *27* (2), 103−111.
(25) Aguado, A.; Bernasconi, L.; Madden, P. A. A Transferable Interatomic Potential for Mgo from Ab Initio Molecular Dynamics. *Chem. Phys. Lett.* **2002**, *356* (5), 437−444.
(26) Henkelman, G.; Arnaldsson, A.; Jónsson, H. A Fast and Robust Algorithm for Bader Decomposition of Charge Density. *Comput. Mater. Sci.* **2006**, *36* (3), 354−360.
(27) Sanville, E.; Kenny, S. D.; Smith, R.; Henkelman, G. Improved Grid-Based Algorithm for Bader Charge Allocation. *J. Comput. Chem.* **2007**, *28* (5), 899−908.
(28) Tang, W.; Sanville, E.; Henkelman, G. A Grid-Based Bader Analysis Algorithm without Lattice Bias. *J. Phys.: Condens. Matter* **2009**, *21* (8), 084204.
(29) Zhang, L.; Han, J.; Wang, H.; Saidi, W.; Car, R.; E, W. *End-to-End Symmetry Preserving Inter-Atomic Potential Energy Model for Finite and Extended Systems*; Curran Associates, Inc., 2018.
(30) Zhang, D.; Bi, H.; Dai, F.-Z.; Jiang, W.; Zhang, L.; Wang, H. DPA-1: Pretraining of Attention-Based Deep Potential Model for Molecular Simulation. *arXiv* 2023, Preprint. DOI: 10.48550/arXiv.2208.08236.
(31) DeePMD-kit. *DeepModeling*. https://docs.deepmodeling.com/projects/deepmd/en/master/model/index.html.
(32) Kresse, G.; Furthmuller, J. Efficient Iterative Schemes for Ab Initio Total-Energy Calculations Using a Plane-Wave Basis Set. *Phys. Rev. B Condens Matter* **1996**, *54* (16), 11169−11186.
(33) Shishkin, M.; Marsman, M.; Kresse, G. Accurate Quasiparticle Spectra from Self-Consistent Gw Calculations with Vertex Corrections. *Phys. Rev. Lett.* **2007**, *99* (24), 246403.
(34) Blochl, P. E. Projector Augmented-Wave Method. *Phys. Rev. B Condens Matter* **1994**, *50* (24), 17953−17979.
(35) Perdew, J. P.; Burke, K.; Ernzerhof, M. Generalized Gradient Approximation Made Simple. *Phys. Rev. Lett.* **1996**, *77* (18), 3865−3868.
(36) Kresse, G.; Joubert, D. From Ultrasoft Pseudopotentials to the Projector Augmented-Wave Method. *Phys. Rev. B* **1999**, *59* (3), 1758−1775.
(37) Osorio-Guillén, J.; Lany, S.; Barabash, S. V.; Zunger, A. Magnetism without Magnetic Ions: Percolation, Exchange, and Formation Energies of Magnetism-Promoting Intrinsic Defects in Cao. *Phys. Rev. Lett.* **2006**, *96* (10), 107203.
(38) Wang, F.; Pang, Z.; Lin, L.; Fang, S.; Dai, Y.; Han, S. Magnetism in Undoped Mgo Studied by Density Functional Theory. *Phys. Rev. B* **2009**, *80* (14), 144424.
(39) Thompson, A. P.; Aktulga, H. M.; Berger, R.; Bolintineanu, D. S.; Brown, W. M.; Crozier, P. S.; in 't Veld, P. J.; Kohlmeyer, A.; Moore, S. G.; Nguyen, T. D.; Shan, R.; Stevens, M. J.; Tranchida, J.; Trott, C.; Plimpton, S. J. Lammps - a Flexible Simulation Tool for Particle-Based Materials Modeling at the Atomic, Meso, and Continuum Scales. *Comput. Phys. Commun.* **2022**, *271*, 108171.


https://doi.org/10.1021/acs.jpclett.4c02934
J. Phys. Chem. Lett. 2025, 16, 31−37